RSC Advances

PAPER

View Article Online
View Journal | View Issue

Cite this: *RSC Adv.*, 2016, **6**, 38972

Facile one-pot scalable strategy to engineer biocidal silver nanocluster assembly on thiolated PVDF membranes for water purification

Maya Sharma,[a] Nagarajan Padmavathy,[b] Sanjay Remanan,[b] Giridhar Madras[c] and Suryasarathi Bose*[b]

Biofouling, due to bacterial growth and colonization, is a significant obstacle in water treatment that severely affects the membrane performance. Nanofiltration effectively removes viruses and other pathogens but is an energy intensive process. Designing and developing low pressure driven membranes with potential antimicrobial and antibiofouling properties is a concern. Under this framework, biocidal silver nanoparticles based polymeric membranes with high content of silver on the membrane surface can control bacterial colonization. However, leaching of silver during water treatment may also lead to toxicity. In the present work, a unique strategy resulting in distinct surface assembly of silver nanoparticles was established on thiol functionalized PVDF membranes. Nanocluster assembly of silver nanoparticles on the PVDF membrane was obtained by esterification reaction between thioglycolic acid (TGA) and alkaline treated PVDF membrane (TGA–PVDF). On the other hand, by introducing thiol–ene chemistry between pentaerythritol tetrakis(3-mercaptopropionate) (PETMP) and alkaline treated PVDF (PETMP–PVDF), well dispersed silver nanoparticles can be tailored on the membrane surface. The silver nanocluster assembly on TGA–PVDF membranes results in control leaching, as confirmed by inductively coupled plasma atomic emission spectroscopy (ICP) and X-ray photon spectroscopy (XPS) analysis in striking contrast to PETMP–PVDF. The trans-membrane flux was assessed and our results uncover that the designed membranes showed higher flux rate. These results have important implications in designing membranes for water purification and reveal the importance of the surface assembly of biocidal nanoparticles towards antibacterial properties.

Received 3rd February 2016
Accepted 8th April 2016

DOI: 10.1039/c6ra03143a

www.rsc.org/advances

Introduction

Many water treatment techniques have been developed and adapted in order to supply safe drinking water.[1] Among them, membrane based filtration devices have been marketed with improved performance. However, membrane lifespan and decrease in flux are the common issues associated with biofouling.[2] Biofouling is the "*Achilles heel*" of the membrane technology because few microbes stay even if most of the population is erased; they grow at the expense of biodegradable substances in the feed water.[3] Among the approaches to eliminate membrane fouling, selection of membrane material with low bacterial affinity or bacteriostatic properties are being explored.[4] The second approach is increasing hydrophilicity of the membrane surface because the biofilm is hydrophobic;[5] it reduces bacterial affinity but does not inhibit the formation of biofilm.

Nevertheless, researchers have attempted surface coating/grafting to incorporate biocidal polymers and antimicrobial/antifouling nanoparticles onto the membrane surface. The surface coating is the simplest way to improve the hydrophilicity of membrane.[6] In addition, surface grafting has also been adopted in which the functional chains such as brushes or layers attached onto the membrane surface through covalent interaction.[7] However, it leads degradation over time. On the other hand, metal nanoparticles like copper, silver *etc.*, have been endowed for fabricating super wetting membranes. Silver, in particular, has been known for its antibacterial activity and is used extensively.[8–10]

Different strategies have been attempted to incorporate silver on polymeric membranes for effective water treatment and to prevent membrane fouling. Taurozzi *et al.*[11] proposed two different pathways to incorporate silver nanoparticles onto polysulfone membrane either by *ex situ* synthesis or *in situ* reduction of silver ions. Recently, Park *et al.*,[12] describe the AgNP–poly(vinylidene fluoride) (Ag–PVDF) membrane nanocomposites with sustainable anti biofouling property through

[a]*Center for Nano Science and Engineering, Indian Institute of Science, Bangalore-560012, India*

[b]*Department of Materials Engineering, Indian Institute of Science, Bangalore-560012, India. E-mail: sbose@materials.iisc.ernet.in*

[c]*Department of Chemical Engineering, Indian Institute of Science, Bangalore-560012, India*

covalent assembly of Ag NPs onto thiol modified polyethylene glycol (PEG) on PVDF membrane. Mauter and co-workers[13] reported polyethylenimine coated silver nanoparticles were electrostatically assembled over negatively charged plasma treated polysulfone membrane. Stable self-assembled polymers have been achieved by growing silver nanoparticles on block copolymer systems such as polyethylene oxide-*b*-polypropylene oxide-*b*-polyethylene oxide (PEO-*b*-PPO-PEO) and polystyrene acrylic acid.[14] Recently, polyacrylic acid (PAA) was grafted on PVDF membrane and silver nanoparticles were loaded.[15] Thus, PVDF has to be invariably blended with hydrophilic polymers or surface cross linkers for effective incorporation of biocidal materials.[16]

Further, these studies do not clearly indicate whether silver is in the form of clusters or monodisperse nanoparticles on these polymeric membranes. Previous reports have typically focused on binding silver with polymer for direct bacterial contact irrespective of the nature of its assembly on the surface.[17] It is believed that the antibacterial activity of silver in its cluster form is different from the dispersed state.[18] The dissolution of silver ions from silver nanoparticles (and subsequent toxicity of Ag^+) is the main mechanism noted in the literature.[19] Silver binds to the bacterial cells through interaction with thiol groups causing cell death. Ionic silver at higher concentrations is toxic against eukaryotic cells, silver in its nanosize shows lower toxicity even at higher concentrations.[20] For instance, nanoparticles (5 and 11 nm diameter) alone were not toxic up to 200 mg L^{-1}.[21]

In light of the existing literature, we report a one-pot, facile approach to develop silver based PVDF membranes. Silver cation is a soft Lewis acid that has an affinity to sulphur and nitrogen.[22] In addition, silver thiolate clusters are known for many applications as biomarkers and optical devices.[23] In the present work, two different thiols have been employed as covalent linkers to decorate silver nanoparticles on the PVDF membrane. Our approach is based on the use of simple thiols like thioglycolic acid (TGA) and pentaerythritol tetrakis(3-mercaptopropionate) (PETMP) on alkaline treated PVDF to produce thiol modified PVDF, on the backbone of PVDF followed by decoration by silver nanoparticles. Surprisingly, TGA directs assembly of silver nanoparticles as clusters while PETMP produced uniform distribution of silver nanoparticles on PVDF membrane. It is envisaged that PETMP suppresses the aggregation of nanoparticles by acting as a "*spacer*" to yield well dispersed silver nanoparticles. This approach is ideally suited for addressing the efficacy of clusters or dispersed silver particles towards antibacterial activity. This study uncovers the importance of silver based PVDF membrane with significant antimicrobial performance with comparable flux efficiency.

Experimental section

Materials and methods

PVDF with M_w 440 000 g mol^{-1} (Kynar 761) was procured from Arkema Inc. Hexadeutero dimethyl sulfoxide (DMSO-d_6 and d_6-acetone for ^{1}H NMR analysis), pentaerythritol tetrakis(3-mercaptopropionate) (PETMP) and polyvinyl pyrrolidone (PVP) coated silver nanoparticles (<100 nm) were obtained from Sigma Aldrich. Azobisisobutyronitrile (AIBN) and thioglycolic acid (TGA) were obtained from Spectrochem, India. *N*,*N*-Dimethylformamide (DMF), isopropanol alcohol, sodium hydroxide (NaOH), LB broth, nutrient agar, sulphuric acid, nitric acid and ethanol were procured from commercial sources and used as received without any further purification.

Preparation of thiol modified PVDF by esterification and thiol–ene chemistry

Required quantity of PVDF powder was treated with a solution containing 1.25 M alcoholic solution of NaOH at 80 °C for 10 minutes. The obtained pale brown powder was washed with deionized water until neutral pH was reached and then dried under vacuum. The functional groups present on PVDF such as OH group[24] and alkene (C=C)[25] can undergo several chemical modifications. This alkaline treated PVDF was then subjected to esterification and thiol–ene reactions, as shown schematically in Fig. 1.

For the esterification reaction, required quantity of alkaline treated PVDF powder was added slowly to the mixture of thioglycolic acid (TGA) and H_2SO_4 in 25 : 1% (v/v). The reaction was continued for 24 h and the thiol terminated PVDF was washed repeatedly with water and subsequently dried under vacuum at room temperature. For thiol–ene reaction involving C=C bond,[26] alkaline treated PVDF was first immersed in a mixture of PETMP/AIBN (6 : 1 mol mol^{-1}) in acetone. The obtained thiol modified PVDF powder was then characterized by NMR.

Fabrication of thiol functionalized PVDF membranes

Non solvent induced phase separation (NIPS) or diffusion induced phase separation (DIPS) or immersion precipitation (IP) is a classical method often employed for preparing porous membranes.[27,28] 25 w/v% of thiol modified PVDF was heated at 50 °C for 1 h in dimethylformamide (DMF). The casting dope was poured on a glass plate and spread using a doctor blade. The doctor blade directs uniform spreading of the dope solution.[28–30] The solution was immersed in the coagulant medium and kept at 4 °C. Casting dope was left for 1 h before pouring to release the bubbles formed during mixing and also to cool down the dope. Water (non-solvent) is usually employed as coagulating medium. The formed membrane (100 ± 10 μm thick) was washed with distilled water to remove excess solvent and subsequently dried under vacuum at 50 °C for 12 h. DMF is highly miscible with water and during this process, the exchange of the solvent in polymer solution with the non-solvent from the coagulation bath results in the phase separation that leads to porous morphology.[31,32] The casting solution was fixed at 25 w/v% after optimizing with different polymer solutions. We found that 25 w/v% PVDF solutions yielded minimum pore size (70 ± 30 nm).

Silver immobilization on thiol-functionalized PVDF membranes

The silver nanoparticles (<100 nm) were covalently bound on to thiolated PVDF membranes (TGA–PVDF and PETMP–PVDF) by

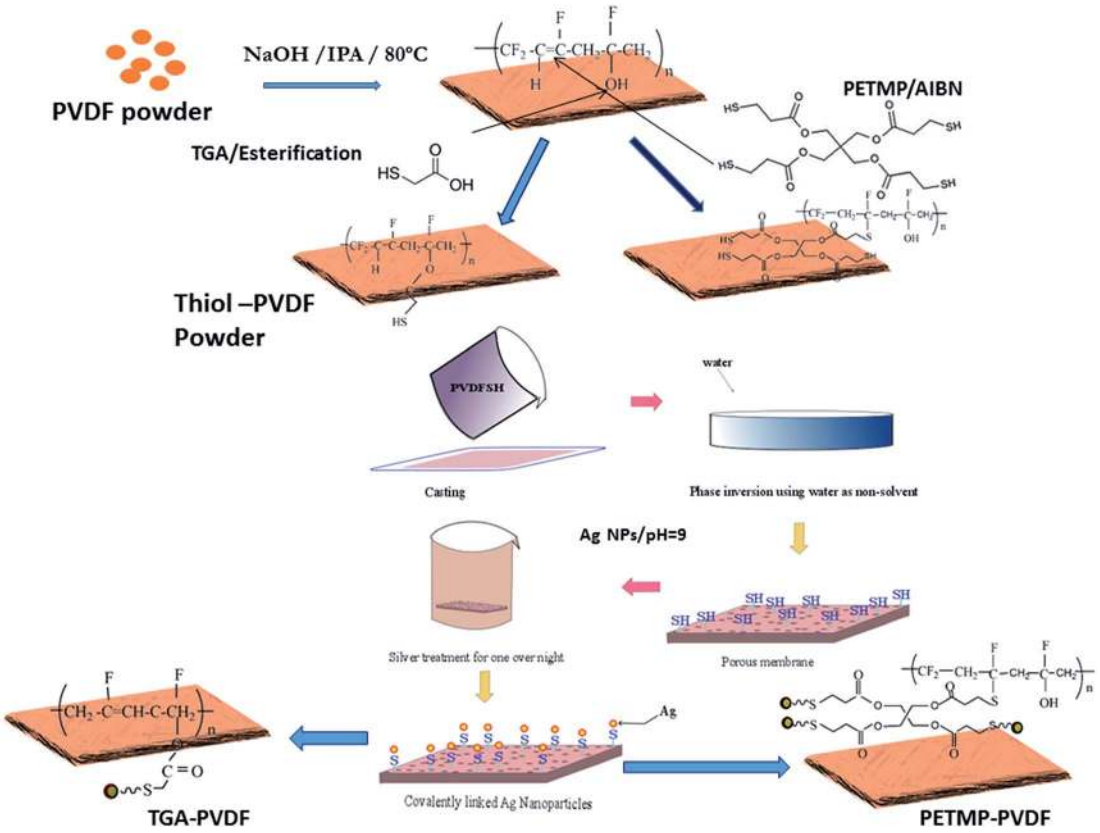

Fig. 1 A cartoon illustrating the fabrication of silver nanoparticles covalently bound on the PVDF membrane *via* esterification and thiol–ene reactions.

suspending the prepared thiolated PVDF membrane (10 × 8 cm^2) into the aqueous solution consisting colloidal silver nanoparticles under mildly basic conditions (pH ~ 9). The solution was then agitated gently at room temperature in an orbital shaker. The membranes were then carefully rinsed several times with distilled water (DI). Silver immobilized TGA modified PVDF membranes were designated as TGA–PVDF, and silver immobilized PETMP modified membranes were designated as PETMP–PVDF.

Characterization of thiol modified PVDF powder

^{1}H Nuclear Magnetic Resonance spectra (^{1}H NMR, Bruker AVANCE 600) were collected on thiol modified PVDF samples using d_6-DMSO and d_6-acetone as solvents.

Characterization of silver treated thiol modified membranes

The surface morphology was analysed using scanning electron microscope (SEM ULTRA 55, FESEM with EDS (Carl Zeiss)). Both upper and lower surfaces were studied for all the designed membranes. The presence of elemental silver in the composite membranes was further confirmed by XPS (Axis Ultra) using an Al monochromatic source (1.486 keV). For quantitative elemental analysis, atomic absorption spectroscopy (AAS, Thermoscientific) was employed wherein a standard calibration curve was prepared using appropriate known concentration of Ag.

Flux measurement

Fig. 2 illustrates schematically an in-house cross flow set up to measure pure water flux.[33,34] It consists of a test cell, reservoir, a booster pump, flow controller and pressure gauges. Membranes of 30 mm diameter were loaded in test cell and measurements were taken from permeate side by a calibrated volume container. The distilled water was pumped using an HPLC pump from a reservoir tank to the membrane unit and the retentate was back flushed.

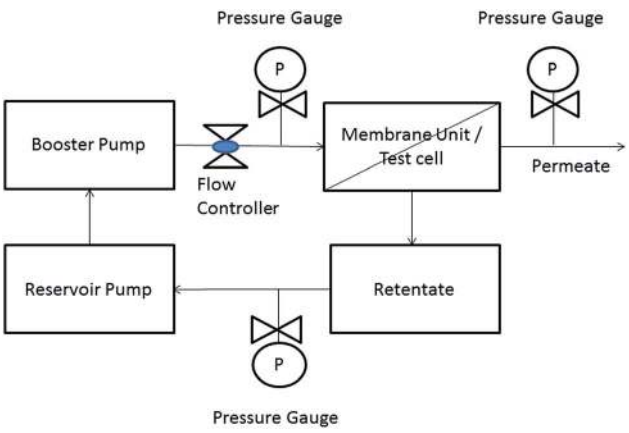

Fig. 2 Schematic of a cross flow cell used for trans-membrane flux studies.

All the experiments were done at room temperature. Membranes were stabilized for 1 h at 15 psi before the readings were taken. For statistical analysis, three replicates were considered. The trans-membrane flux (J_w) was calculated using the following equation,

$$J_w = \frac{V}{At} \quad (1)$$

where, A is the effective area of the membrane and t is the flow time for permeate to fill volume V. The unit was cleaned with ethanol to avoid bacterial contamination and distilled water was used for the experiments.

Membrane porosity

Membrane porosity was estimated gravimetrically. The oven-dried PVDF membrane sample was cut, weighed and subsequently submerged in a 50 mL container filled with distilled water for 1 h. The porosity (ε) was then calculated by measuring the difference in weight before and after the sample wetting using the following equation,

$$\varepsilon = \frac{m_{wet} - m_{dry}}{\rho_{water} V_s} \quad (2)$$

In eqn (2), m_{wet} and m_{dry} is the wet and dry weight of the membrane respectively. ρ_{water} is the density of the water, V_s is the sample volume. A detailed discussion of porosity calculation is available elsewhere.[35,36]

Contact angle measurement

Water contact angle of the composite membranes was calculated using water drop method (OCA, 15EC, data physics). DI water (0.1 mL) was used to estimate the contact angle using sessile drop approach. Image was captured after 1 min. For each composite membrane, the experiments were repeated with three replicates. The contact angles were calculated with the help of the software.

Silver leaching experiments

Inductively coupled plasma-optical emission spectroscopy (ICP-OES, Thermo-iCAP 6000) was used to quantify the release of silver ions. The membranes were incubated at 37 °C for 3 h in 1 mL DI water. The solution containing silver ions eluted from the membranes was diluted prior to quantification. Final concentration was quantified using a set of single-element external calibration standards to enable measurements in the 0–1 ppm concentration range.

Antibacterial efficiency of modified thiol membranes

Standard plate count method was used to test the antibacterial property of the composite membranes. *Escherichia coli* (Gram-negative bacteria, strain 25922 ATCC) was grown in 100 mL of sterile Luria Broth (LB) at 37 °C for 6 h and harvested in the log phase. Optical density (OD) of bacteria culture was set to 0.5 at 600 nm. Before starting the experiments, bacteria culture was re-suspended in isotonic 0.9% saline solution to reach a concentration of 10^7 CFU mL^{-1}. The suspended bacteria culture (1 mL) was then added to the composites membranes and incubated at 37 °C for 3 h. The unmodified neat PVDF membranes were taken as control samples. To examine the bactericidal and antifouling properties, supernatant was used for the standard plate count test. 100 μL of supernatant was further serial diluted and cultured in nutrient agar, then incubated at 37 °C for another 18 h. Three replicates were used for each sample. *E. coli* colonies grown on agar plate were photographed and for quantitative analysis, the number of viable bacterial colonies was counted for different dilutions. To analyze the attached bacterial cells on composite membranes, the membrane surface was rinsed with saline solution and fixed with 3.7% formaldehyde solution for 20 min. Membrane surface was again rinsed with saline solution to remove the extra formaldehyde. Prior to SEM imaging, membranes were dehydrated using ethanol. Samples were gold sputtered prior to imaging.

The effect of biofouling on the permeate flux was assessed using *E. coli* as a biofoulant. Optical density (OD) of bacteria LB culture was set to 0.5 at 600 nm. The bacteria culture was re-suspended in isotonic 0.9% saline solution to reach a concentration of 10^7 CFU mL^{-1} appropriately. The prepared *E. coli* suspension solution ($\sim 10^7$ CFU mL^{-1}) was used as feed solution and passed through membranes using the aforementioned flux setup for 8 h. The flux was recorded after each hour. After 8 h, the membranes were sonicated with DI water for 5 min. The membranes were subsequently fixed with 3.7% formaldehyde solution for 20 min. Membrane surface was again rinsed with saline solution to remove the excess formaldehyde. Standard procedure was followed for SEM imaging. To analyze the presence of *E. coli* in permeate, the permeate water was collected in sterilized sealed tubes and was used in standard plate count. 100 μL of supernatant was further serial diluted, was cultured in nutrient agar, and incubated at 37 °C for another 18 h. *E. coli* colonies grown on agar plate was photographed and for quantitative analysis, the number of viable bacterial colonies was counted for different dilutions.

Results and discussion

Tailored PVDF surface to immobilize silver nanoparticles/clusters

The modification of PVDF backbone by thiol groups stems from the alkaline treatment. The alkaline treatment in the presence of alcohol results in dehydrofluorination thereby yielding hydroxyl and C=C bonds on the backbone.[37] The OH group is introduced during the elimination reaction of one of the fluoride anions from CF_2.[37] These functional groups can further be modified through esterification and thiol–ene reactions by TGA and PETMP respectively. The thiol–ene reaction was selected because of its high reaction efficiency. Introducing –SH group on PVDF surface is usually carried out either by dipping PVDF membranes in thiol solution or blending PVDF with hydrophilic polymers such as PEG[12] following by thiol modification. These methods require not only extensive reaction steps but also results in excess thiol groups on the surface. In our case, each

PVDF segment contains only one –SH group imparted either through esterification or thiol–ene reactions (see Fig. 1). Sulphur groups readily react with bases, acid, ketones or halogens; while the carboxylic acid (of thioglycolic acid) will specifically react in the presence of alcohol or amines.[38] The hydroxyl groups present on the PVDF reacts with the carboxylic acid of TGA thereby producing thiol linker on PVDF. The reaction of thiol and alkenes is an efficient method for the rapid production of crosslinked polymer networks using mercaptopropionate.

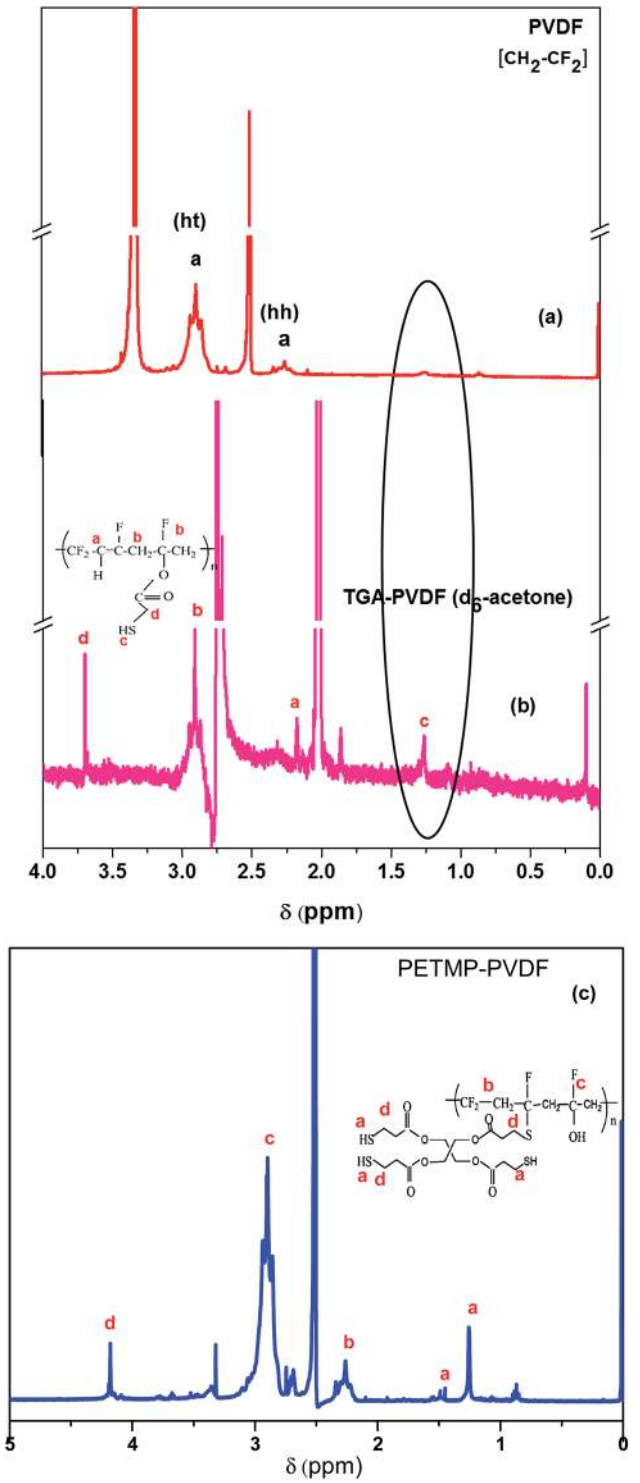

Fig. 3 ^{1}H NMR spectra of PVDF (a), thiol modified TGA–PVDF, PETMP–PVDF samples (b and c). The spectrum was taken on the powder in deuterated DMSO and acetone.

A closer look of TGA–PVDF samples using SEM (discussed later) revealed silver nanoclusters on the membrane surface. It can be explained based on the concept of the formation of thiol silver clusters. In contrast, in the case of PETMP–PVDF sample, no such clusters were observed; rather an even distribution of silver nanoparticles was noticed. PETMP acts as a "*spacer*" for the silver nanoparticles and prohibit aggregation and results in a uniform distribution on the membrane surface.

^{1}H NMR spectra of PVDF, TGA–PVDF and PETMP–PVDF are shown in Fig. 3. The PVDF spectrum (Fig. 3a) exhibits two signature peaks *i.e.* head to-tail and head-to-head arrangements in the region of 2.89 (t, $-CF_2CH_2-CF_2CH_2-$ head-to-tail); 2.3 (t, $-CF_2CH_2-CH_2CF_2-$ tail-to-tail) respectively. In TGA–PVDF (Fig. 3b), along with PVDF signature peaks, the chemical shift at 1.26 ppm is assigned to mercaptan proton (SH) and the resonance at 3.69 ppm is meant for methylene protons of thioglycolic acid (TGA). In Fig. 3c (PETMP–PVDF), shift at 1.26–1.45 ppm (s, SH) and 4.17 ppm due to $-CH_2-O-$ of PETMP appear along with PVDF signals.[39] ^{1}H NMR (400 MHz, DMSO-d_6, δ/ppm): pristine PVDF, 2.89 (t, $-CF_2CH_2-CF_2CH_2-$ head-to-tail); 2.3 (t, $-CF_2CH_2-CH_2CF_2-$ tail-to-tail). TGA–PVDF (acetone-d_6, δ/ppm): 2.90 (head-to-tail, PVDF); 2.18 (t, tail-to-tail, PVDF); 1.26 (s, mercaptan (SH)); 3.69 (s, CH_2 proton of thioglycolic acid). PETMP–PVDF (DMSO-d_6, δ/ppm): 2.89 (head-to-tail, PVDF); 2.26 (t, tail-to-tail, PVDF); 1.26–1.45 (s, SH); 4.17 ppm due to $-CH_2-O-$ of PETMP. The spectra further confirmed the presence of free thiol groups which can further be utilized, in the next step, to anchor silver nanoparticles.

The presence of silver and sulphur on thiolated PVDF membrane surfaces has been further confirmed by X-ray photoelectron spectroscopy (XPS) (Fig. 4). These surfaces are thoroughly washed with ethanol and dried by N_2 purging before collecting the XPS data. This washing procedure eliminates the possibility of the presence of physisorbed thiols and excess silver ions on the surface. Fig. 4a and b depict S 2p spectra of TGA–PVDF and PETMP–PVDF membranes, respectively. A peak positioned at 162.3 eV in TGA–PVDF is assigned to surface bound Ag–thiolate system.[39] Based on Pearson's rule, the sulfur atom in a thiol group and a noble metal tend to share the valence electrons to form a covalent bond. Mildly basic conditions, therefore, favoured deprotonation of alkyl thiol and the formation of covalent bonds between the colloidal AgNPs.[40] In PETMP–PVDF (Fig. 4b), the peak fitting indicates two peaks positioned at 162 eV and 167.2 eV. The peak at 162 eV corresponds to the Ag–thiolate and higher binding energy peak observed at 167.2 eV is a direct evidence of the strong interaction of sulphur and carbon.[41] We did not observe any free thiol in XPS spectra, in both the cases of TGA–PVDF and PETMP–PVDF membranes which indicate the thiols reacted effectively with Ag nanoparticles.

Fig. 4c and d show XPS profiles of Ag 3d region for TGA–PVDF and PETMP–PVDF respectively. After immobilization of

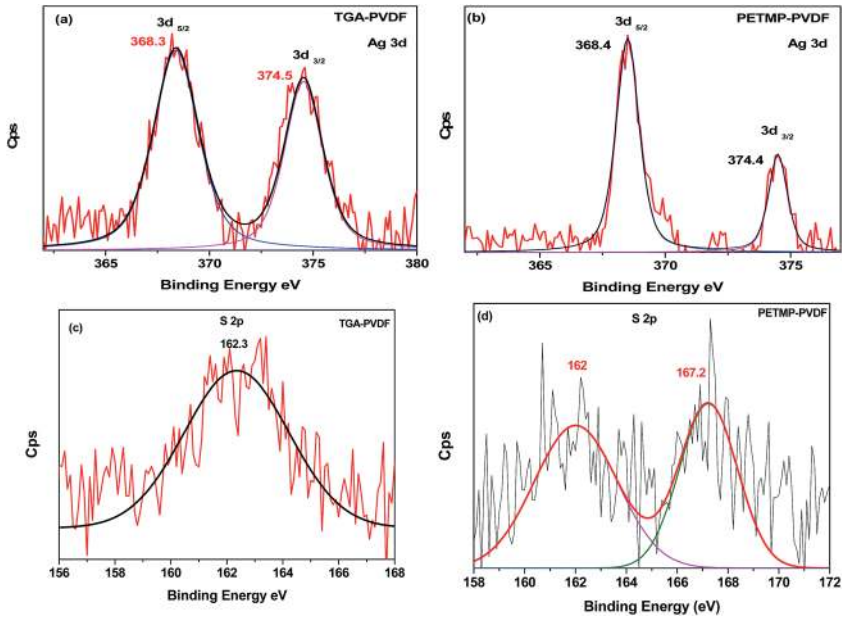

Fig. 4 (a and b) XPS spectra of S 2p region for (a) TGA–PVDF and (b) PETMP–PVDF (c and d) XPS profile of Ag-3d region for (c) TGA–PVDF membrane (d) PETMP–PVDF membrane.

Ag nanoparticles with thiolated PVDF membranes, the formation of S–Ag bonds are clearly visible at 368.3 eV and 368.4 of Ag $3d_{5/2}$ of TGA–PVDF and PETMP–PVDF respectively. The silver nanoparticles on the membrane surface therefore appeared to be in their elemental state instead of any silver based complex.[42] It is in good agreement with literature reports for silver complexes with thiol based ligands bound to metals through Ag–S bonds.[43]

Morphology of membrane surface

The membrane surface morphology (before and after modification of PVDF) was observed by SEM, as shown in Fig. 5. All the membranes showed a dense skin layer on the top surface. The surface average pore size is *ca.* 70 ± 30 nm (Fig. $5a_1$) whereas cross sectional SEM showed average pore size of 300 ± 50 nm with finger like projections on one side (Fig. $5a_2$). The smaller pore size on surface is attributed to high dope solution concentration (25 wt% PVDF). As the dope concentration was reduced, the overall membrane pore size increased (not shown here). The top and bottom surfaces of the membrane showed entirely distinct morphologies which is consistent with the reported literatures. The top surface is usually less globular, porous and show high integrity, the bottom surface filled with globular structure.[44] Here, we considered only the top surface as the active area for further experiments. The SEM micrographs of TGA–PVDF membranes showed the existence of silver nanoparticles attached on the membrane surface (Fig. 5b).

As it is evident from surface morphology, that silver nanoparticles are well distributed on the membrane surface but assemble as clusters. This can be attributed to a breakdown of the electronically repulsive stabilizing structure of silver nanoparticles by introducing the covalent linkage between Ag and SH and a subsequent aggregation of silver nanoparticles on the surface of the membrane. The EDS spectra on the TGA–PVDF membranes revealed the existence of silver nanoparticles on the membrane surface. Surface characteristics like pore size, pore structure of TGA–PVDF is similar to that of neat PVDF membranes. As TGA is a small molecule, the inherent PVDF membrane characteristics do not alter significantly with silver immobilization on the surface. The SEM micrographs of top surface of PETMP–PVDF membranes are shown in Fig. 5c. The PETMP–PVDF membranes showed a different kind of morphology in striking contrast to PVDF and TGA–PVDF membranes. The top surface of PETMP–PVDF membranes showed open, globular porous morphology, but the pores are not apparent in the SEM micrographs. The EDS spectrum further confirms the existence of silver nanoparticles on the membrane surface. Apart from Ag, free sulphur is also present in the EDS spectra which indicate the presence of PETMP molecules on the membranes. The different morphology of PETMP–PVDF membranes can be ascribed to the covalent linkage of PETMP molecule onto PVDF that alters the crystallization kinetics of PVDF. Intriguingly, the silver nanoparticles are uniformly distributed on the membrane surface, as the particles are covalently attached to –SH facilitated by PETMP molecule. The porosity results are in corroboration with surface morphologies as discussed in the next section.

Permeate flux through modified membranes

Porosity of different membranes, estimated by gravimetric method, is shown in Fig. 6a. The porosity of the membranes decreased in the modified membranes. For instance, the PETMP–PVDF showed the least porosity of 35% whereas the neat PVDF membranes showed the highest porosity of 81%. The

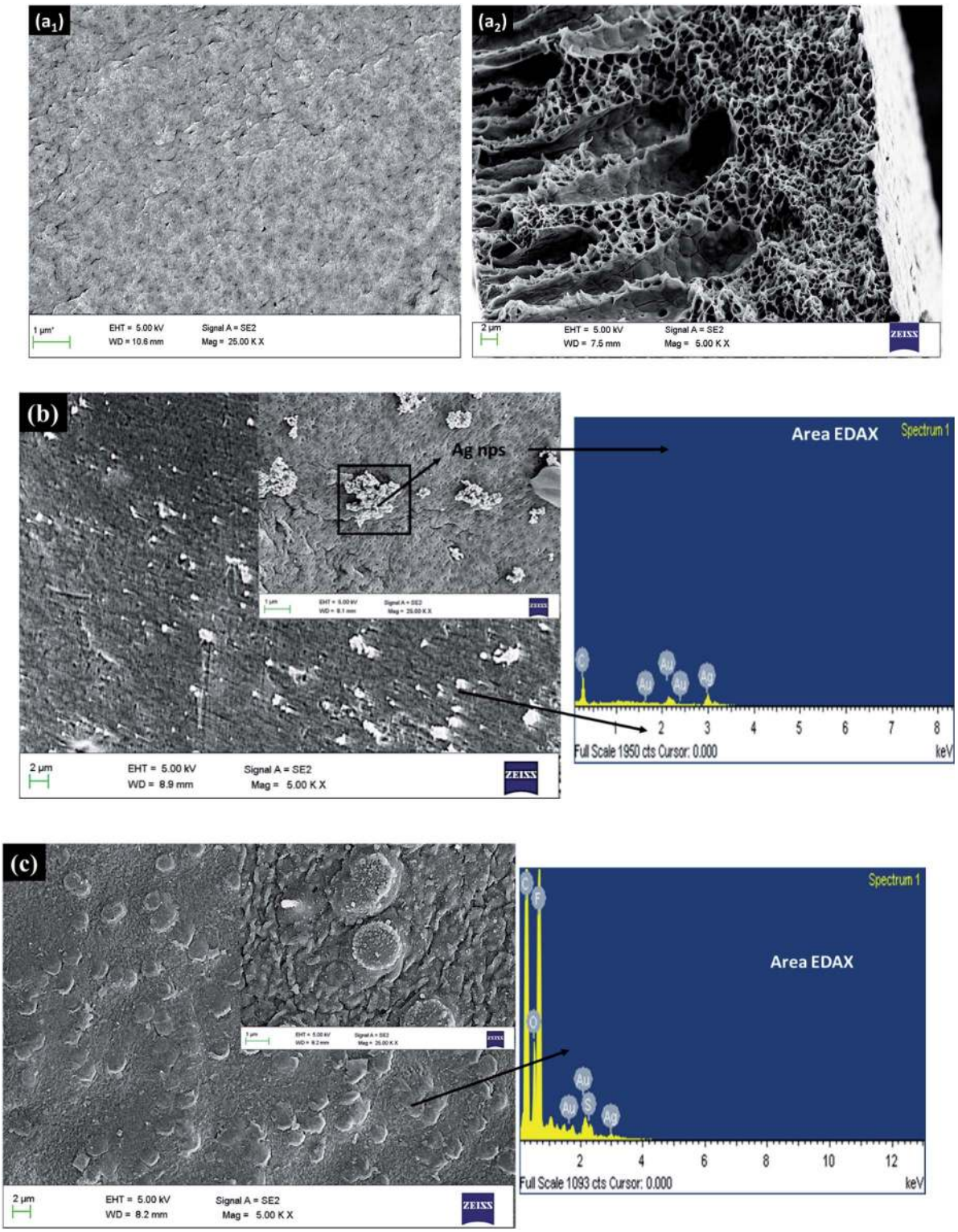

Fig. 5 SEM images of (a) pristine PVDF membrane (b) TGA–PVDF (c) PETMP–PVDF membrane (the inset in (b) and (c) illustrates a magnified image showing the silver nanoclusters and particles on the surface. In addition, the inset also depicts the corresponding EDS).

lower porosity of PETMP–PVDF membranes can be attributed to the less pore size of these membranes. While the porosity is linearly related to permeate flux, the less porous PETMP–PVDF led to lower flux and will be discussed more detail in the next section.

The as prepared membranes were subjected to a constant transmembrane pressure of 15 psi for 60 min till a steady flux was attained. The transmembrane water flux for all membranes at 10 psi was calculated using eqn (1) and is shown in Fig. 6b. All the membranes showed linear dependence of water flux on the

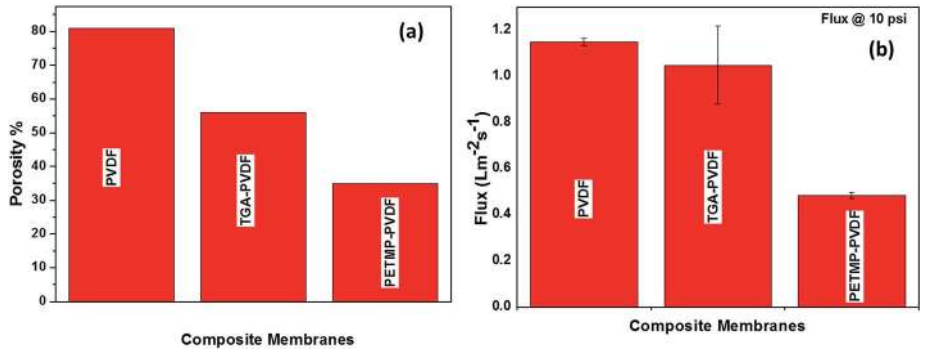

Fig. 6 (a) Porosity of all PVDF based membranes, (b) transmembrane flux calculated at 10 psi for all membranes.

applied transmembrane pressure (not shown here). It is evident from Fig. 6b that neat PVDF membranes showed higher pure water permeate flux as compared to TGA–PVDF and PETMP–PVDF membranes. The higher flux for PVDF membranes can be ascribed to high porosity of these membranes. From SEM (Fig. 5a$_2$), it is clear that PVDF membranes showed uniform distribution of pores throughout the membrane surface. The TGA–PVDF membranes showed similar permeate flux (1.04 L m^{-2} s^{-1}) as that of neat PVDF (1.14 L m^{-2} s^{-1}). This can be attributed to the similar morphology and porosity in these membranes. From EDS and AAS, it is evident that silver concentration in TGA–PVDF samples is significantly less (1.8 atomic%) which does not alter the membrane porous structure. The pure water flux was obtained lowest for the PETMP–PVDF membranes (0.48 L m^{-2} s^{-1}). The lower flux can be due to lesser porosity in these membranes.

Contact angle measurements

The average water contact angles for all prepared membranes surfaces are shown in Fig. 7a. The surface contact angle for neat PVDF membrane is *ca.* 89° which is in agreement with the hydrophobic nature of PVDF.[45,46] After thiol treatment, the contact angle of the membrane has decreased especially with PETMP treatment (*ca.* 61°). It is envisaged that contact angle depends on many parameters like surface chemistry, roughness, *etc.*[47] The comparatively lower surface contact angle for PETMP–PVDF membranes can be due to high surface roughness of the membranes. The high hydrophilicity of PETMP–

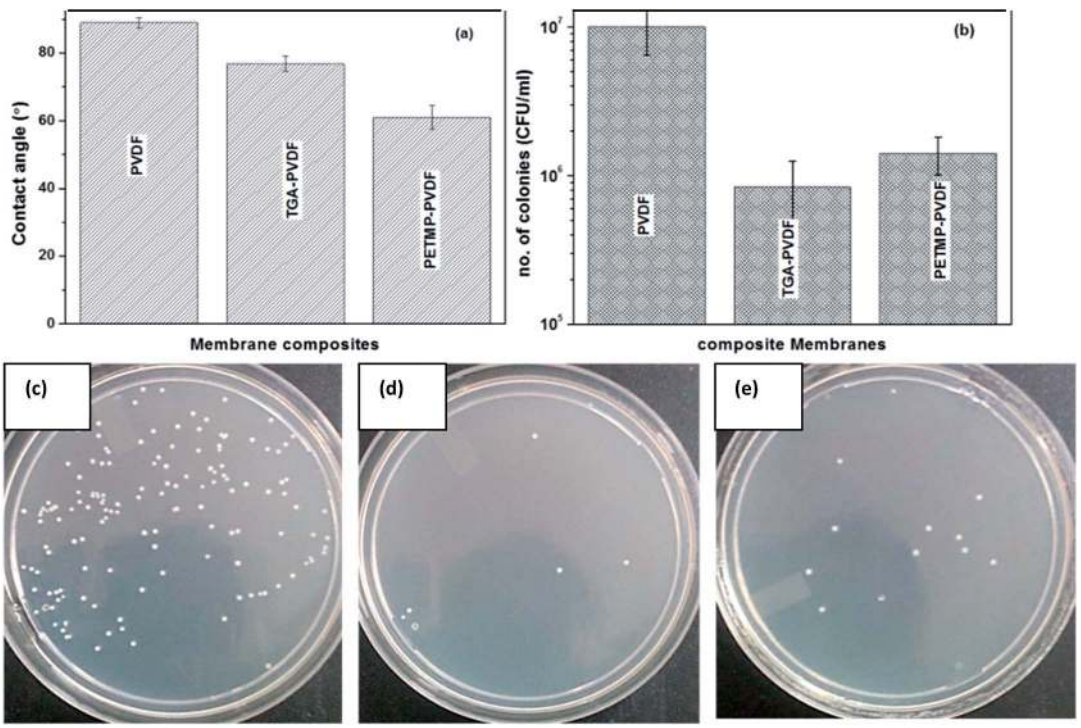

Fig. 7 (a) Water contact angle of the designed membranes, (b) quantitative antibacterial activity of membranes in terms of CFU mL^{-1}. The bottom images of agar plates showing bacterial colonies for (c) neat PVDF membrane, (d) TGA–PVDF membrane, and (e) PETMP–PVDF membrane.

PVDF membrane can possibly be due to the presence of significant amount of silver nanoparticles on the treated PVDF. Silver nanoparticles can release silver ions in aqueous phase by oxidation and silver ions can simultaneously be adsorbed on the silver nanoparticles surface. It leads to a hydrated silver ion that is the probable source of silver nanoparticles hydrophilicity.[48] Dissolved oxygen present in the aqueous media of *ca.* 10 ppm is rather sufficient for silver oxidation. The PETMP–PVDF membrane exhibited higher content of silver (by XPS and ICP data) resulting in a more hydrophilic membrane based on the above concept compared to TGA–PVDF membrane.

Antibacterial and antifouling properties in the membranes

Standard plate count method was used to characterize antibacterial nature of these composite membranes. *Escherichia coli* (*E. coli*) was chosen as a model bacterium because it is widely known contaminant in the drinking water and cause serious health ailments. Apart from medical illness, *E. coli* is also known to form biofilms on almost all hydrated surfaces.[49] The biofilm formation (biofouling) results in deterioration of flux due to the formation of a low permeability biofilm on the membrane surface.[50] PVDF surface is prone to biofouling due to physicochemical and electrostatic interactions between the bacterial and PVDF surfaces.[51] Fig. 7b–e shows the number of bacterial colonies grown on agar plates for different composite membranes, where approximately 10^7 CFU mL^{-1} of initial concentration was used in the experiment. The modified composite membranes show fewer colonies than control (PVDF) membranes. After 3 h of incubation, TGA–PVDF membranes showed 95% decrease in bacteria colonies as compared to PVDF. PETMP–PVDF composite membranes also showed significant decrease in colonies *i.e. ca.* 87% less than the control samples. It is noteworthy that although PETMP–PVDF composite membranes contain higher concentration of silver (from EDS and AAS). TGA–PVDF membranes showed better bactericidal effects. This can be attributed to better leaching of silver in the TGA–PVDF composites as discussed in next section. This clearly indicates that TGA–PVDF composites are bactericidal as well as prevent biofouling. The quantitative results of bacteria colonies on the different membranes are shown in Fig. 7b. It is evident that TGA–PVDF membranes show less bacterial colonies as compared to PETMP–PVDF and neat PVDF membranes. The TGA–PVDF membranes showed significant reduction in bacterial colonies as illustrated in Fig. 7b–d.

SEM microscopy was employed to gain more insight in the biofilm formation on membrane surface as shown in Fig. 8.

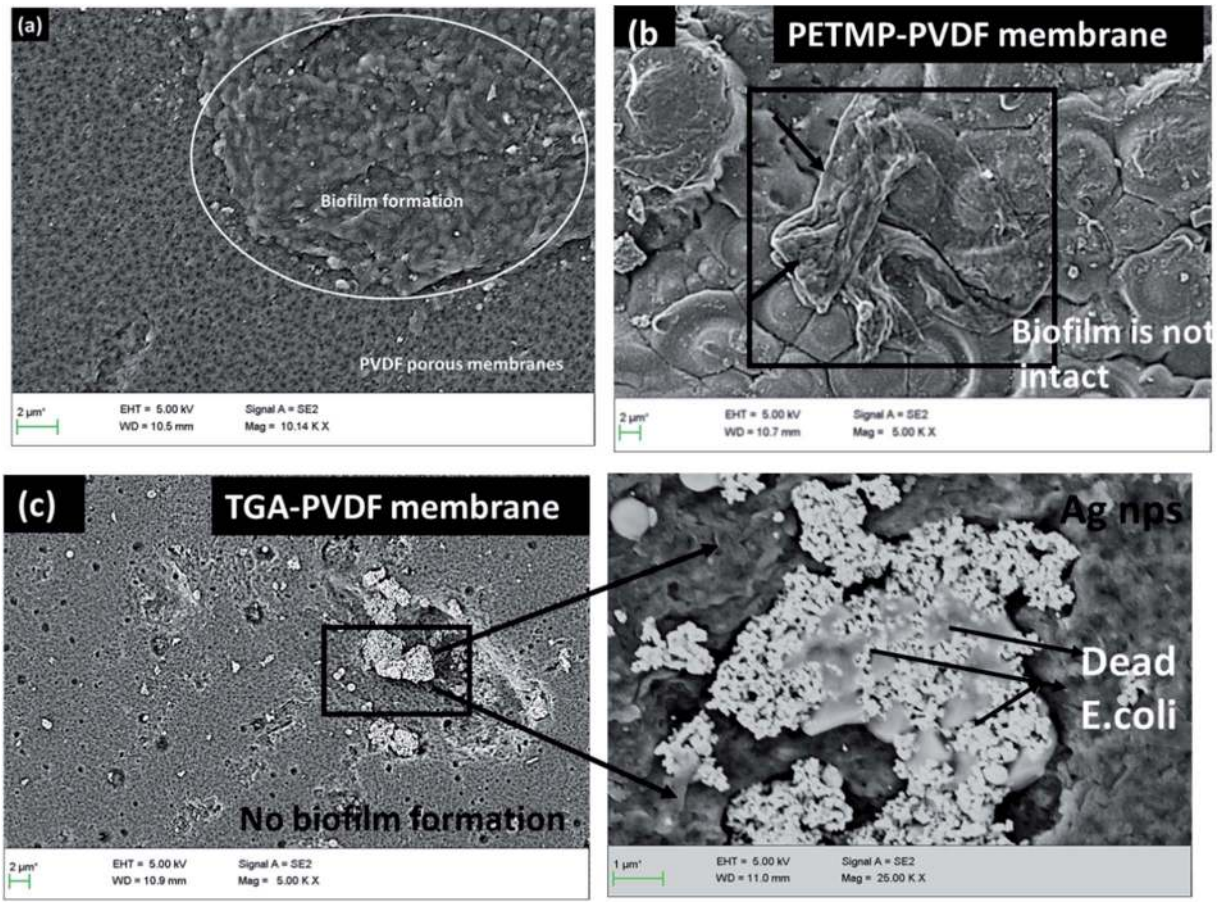

Fig. 8 Scanning electron microscopy of (a) neat PVDF membranes showing biofilm formation after 3 h of incubation, (b) PETMP–PVDF membranes with disrupted biofilm after 3 h of incubation, (c) TGA–PVDF membranes with no biofilm after 3 h incubation (inset showing dead *E. coli* bacteria around the silver nanoclusters).

Biofilm was observed on the PVDF membranes which signify bacterial adhesion on the membrane surface (Fig. 8a). Interestingly, membranes with PETMP also showed curled bacterial colonies in the SEM images (Fig. 8b). This can be due to the high surface roughness of the PETMP–PVDF composite membranes which is also supported by lower contact angle. It is noteworthy that even though PETMP–PVDF membranes are hydrophilic and prone to bacterial adhesion, we can realize that the biofilm is not intact in these samples. At most of the places on the membrane surface (not shown here), the biofilm was not intact. This is attributed to the bactericidal effects of silver nanoparticles present on the membrane surface. As leaching of silver is not very prominent in PETMP–PVDF membranes, due to covalent linkages the antibacterial effects were well discussed. The inhibition effect of silver ions on microorganism has been well studied but the exact mechanism is not fully known. It is believed that silver ions inactivate the DNA replication and formation of cellular proteins,[52] and also cause protein denaturation.[53] Interestingly, there was no such biofilm on TGA–PVDF composite membranes (Fig. 8c). In the enlarged micrograph, we can clearly see dead bacterial cells present on the surface. These results are in accordance with the plate count results where TGA–PVDF composite membrane showed maximum bactericidal activity. The reduction in colony count and antifouling properties of TGA–PVDF membranes is ascribed to the presence of silver clusters on the composite membrane surface.

The silver ions are positively charged whereas the *E. coli* membrane is negatively charged. The electrostatic interactions between the microbe membrane and positively charged nanoparticles is crucial for the inactivity of bacterial colonies.[54] In our recent work on PE/PEO blends with GO–NH_2, the antibacterial efficiency of the membrane was attributed to the ROS (reacting oxygen species) and physical damage induced by rough GO surface.[33] The results from plate count and SEM clearly indicate that TGA–PVDF membrane was the most effective among the three membranes designed in this work.

Silver ions leaching from modified membranes

The leaching of Ag^+ from modified membranes was confirmed by ICP analysis. The released Ag^+ concentration from the PETMP–PVDF is lower compared to TGA–PVDF membranes. After 3 h, the TGA–PVDF membranes showed higher release of Ag^+ (68 ppb) than that of PETMP–PVDF membranes (14 ppb). It is worth mentioning that during the experiment, similar sample size was maintained. These indicate the gradual release of silver from the membranes, but as the release is very slow, the lifetime of membranes are quite high. The main bactericidal mechanism in these membranes is Ag^+–bacteria interactions.[55] The antimicrobial properties of the modified membrane were ascribed to the leaching of Ag^+ from the membranes.[56,57] Our results infer that Ag^+ is the main molecular toxicant that leads to high antimicrobial activity. These results also support our findings that TGA–PVDF membranes are better antimicrobial agents than PETMP–PVDF membranes. Hence, our findings uncover the importance of silver nanocluster in rendering bactericidal properties of the designed membranes.

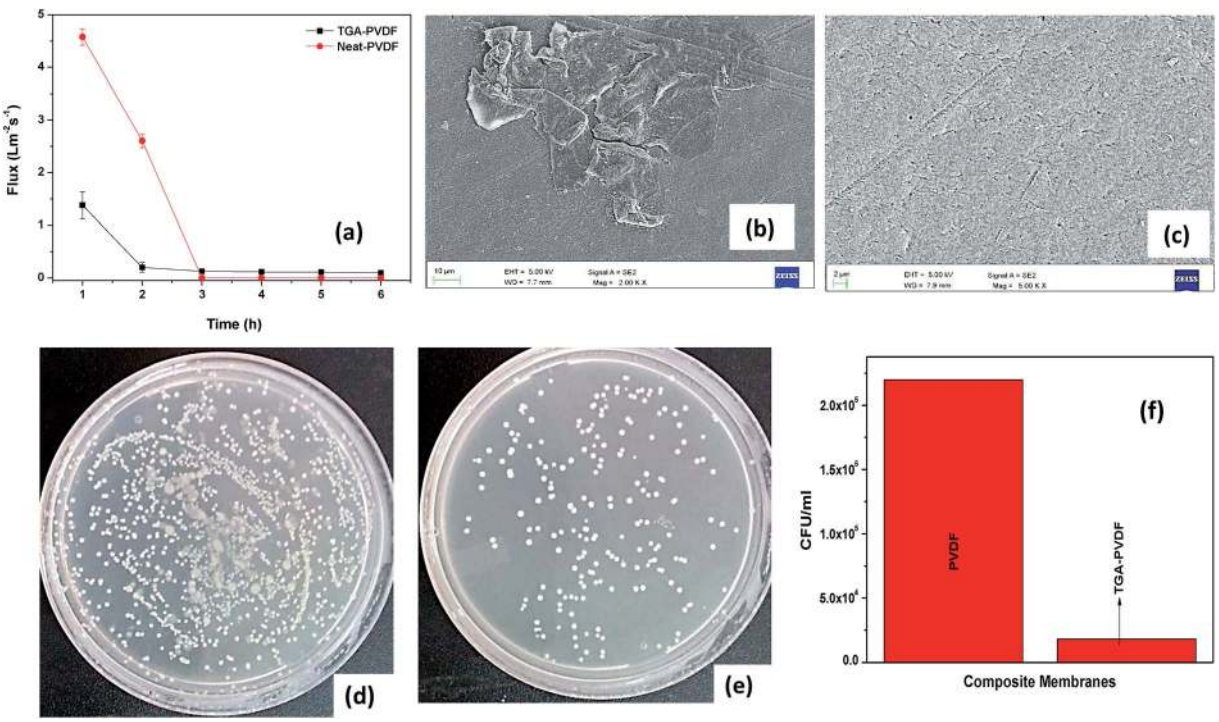

Fig. 9 (a) Permeate flux after 8 h with TGA–PVDF and control PVDF membrane (b); (c) SEM images of TGA–PVDF and PVDF after flux measurement respectively (d); (e) corresponding bacterial colonies obtained after plating the permeate and; (f) CFU mL^{-1} of PVDF and TGA–PVDF membranes.

We further tested the biofouling on the composite PVDF membranes using *E. coli* as a biofoulant. Thus far, we established that TGA–PVDF membranes have better bactericidal properties than the other counterparts. The biofouling experiments were done with TGA–PVDF and PVDF membranes only. Transmembrane permeate flux for composite membranes with time (for 8 h) was measured at 10 psi as shown in Fig. 9a. It is evident that in the initial 2 h, neat PVDF membranes showed higher water permeate flux as compared to TGA–PVDF membranes. The higher flux for PVDF membranes can be ascribed to higher porosity of these membranes. Water flux becomes almost zero for PVDF membranes after 3 h, which indicates biofouling on the membranes. Water flux gradually decreased with time for TGA–PVDF membranes in the initial 3 h and subsequently it becomes constant for the next 5 h. These findings clearly indicate better performance of TGA–PVDF membranes as compared to PVDF. These results were attributed to the suppression of microorganism adhesion and growth due to the biocidal properties of the TGA–PVDF composite membrane. The membranes obtained after the flux measurements were monitored using SEM (Fig. 9b and c). It is seen that no adhered biofilm was present on the TGA–PVDF membrane. On the contrary, biofilm was observed on the neat PVDF membrane surface. Fig. 9d and e shows the number of bacterial colonies grown on agar plates, when permeate water was used for plating. The TGA–PVDF membranes showed significantly fewer colonies than PVDF membranes. After 8 h, the PVDF membranes showed 2×10^5 CFU mL^{-1}. On the other hand, the TGA–PVDF membranes showed significant reduction in colonies (1.8×10^3 CFU mL^{-1}). This clearly indicates that TGA–PVDF membranes are antimicrobial and prevent biofouling on the surface. The quantitative results of bacteria colonies on the studied membranes are shown in Fig. 9f. It is well evident that TGA–PVDF membranes showed less bacterial colonies as compared to the neat PVDF membranes. This facile one-pot approach with improved flux, antibacterial and antifouling properties can open new avenues in separation technology especially for water purification.

Conclusions

Our results uncover an important observation related to the surface assembly of biocidal nanoparticles on polymeric membranes. PVDF can be modified by alkaline treatment and further surface architecture can be engineered by selecting a specific thiol compound. For instance, by modifying the PVDF with TGA and PETMP, different surface assembly of silver nanoparticles can be tailored. This is clearly evident from the electron microscopy and selective area EDS scans. Our results clearly show that a specific thiol compound direct the silver nanoparticles assembly on the designed membranes. It is now understood that PETMP acts like a "*spacer*" and impedes nanoparticle aggregation whereas, silver nanocluster assembly was observed in the case of TGA–PVDF. The biofilm formation was distinctly suppressed in TGA–PVDF membrane. The ICP analysis revealed that Ag^+ released from the membrane surface assisted in rendering antibacterial surface. Our findings will help guide researchers involved in designing water filtration membranes and also help in understanding the effect of surface assembly of biocidal nanoparticles towards antibacterial properties.

Acknowledgements

Authors would like to acknowledge Department of Science and Technology, DST and the Indian National Science Academy (INSA) for the financial support. Authors are grateful to Prof. S. Subramanian, Department of Materials Engineering, IISc, for extending his AAS facility. NP thanks Prof. Kaushik Chatterjee for the postdoctoral funding. Authors would also like to acknowledge MNCF, CeNSe, NMR facilities, SID, IISc, for characterization facilities. Giridhar Madras thanks DST India for J. C. Bose fellowship.

References

1 F. Liu, N. A. Hashim, Y. Liu, M. R. M. Abed and K. Li, *J. Membr. Sci.*, 2011, **375**, 1–27.
2 J. A. Brydson, in *Plastics Materials*, ed. J. A. Brydson, Butterworth-Heinemann, Oxford, 7th edn, 1999, pp. 363–385, DOI: 10.1016/b978-075064132-6/50054-1.
3 H. C. Flemming, G. Schaule, T. Griebe, J. Schmitt and A. Tamachkiarowa, *Desalination*, 1997, **113**, 215–225.
4 N. Hilal, L. Al-Khatib, B. P. Atkin, V. Kochkodan and N. Potapchenko, *Desalination*, 2003, **158**, 65–72.
5 H.-C. Flemming and J. Wingender, *Nat. Rev. Microbiol.*, 2010, **8**, 623–633.
6 B. Van der Bruggen, *J. Appl. Polym. Sci.*, 2009, **114**, 630–642.
7 J.-H. Kim and K.-H. Lee, *J. Membr. Sci.*, 1998, **138**, 153–163.
8 A. Dror-Ehre, H. Mamane, T. Belenkova, G. Markovich and A. Adin, *J. Colloid Interface Sci.*, 2009, **339**, 521–526.
9 D. Gangadharan, K. Harshvardan, G. Gnanasekar, D. Dixit, K. M. Popat and P. S. Anand, *Water Res.*, 2010, **44**, 5481–5487.
10 V. Sherly Arputha Kiruba, A. Dakshinamurthy, P. S. Subramanian and P. Mosae Selvakumar, *J. Exp. Nanosci.*, 2015, **10**, 532–544.
11 J. S. Taurozzi, H. Arul, V. Z. Bosak, A. F. Burban, T. C. Voice, M. L. Bruening and V. V. Tarabara, *J. Membr. Sci.*, 2008, **325**, 58–68.
12 S. Y. Park, J. W. Chung, Y. K. Chae and S.-Y. Kwak, *ACS Appl. Mater. Interfaces*, 2013, **5**, 10705–10714.
13 M. S. Mauter, Y. Wang, K. C. Okemgbo, C. O. Osuji, E. P. Giannelis and M. Elimelech, *ACS Appl. Mater. Interfaces*, 2011, **3**, 2861–2868.
14 A. V. Perdikaki, P. Tsitoura, E. C. Vermisoglou, N. K. Kanellopoulos and G. N. Karanikolos, *Langmuir*, 2013, **29**, 11479–11488.
15 J.-H. Li, X.-S. Shao, Q. Zhou, M.-Z. Li and Q.-Q. Zhang, *Appl. Surf. Sci.*, 2013, **265**, 663–670.
16 W. Zhang, Y. Zhu, X. Liu, D. Wang, J. Li, L. Jiang and J. Jin, *Angew. Chem., Int. Ed.*, 2014, **53**, 856–860.
17 A. Ivask, A. ElBadawy, C. Kaweeteerawat, D. Boren, H. Fischer, Z. Ji, C. H. Chang, R. Liu, T. Tolaymat,

D. Telesca, J. I. Zink, Y. Cohen, P. A. Holden and H. A. Godwin, *ACS Nano*, 2014, **8**, 374–386.
18 S. Chernousova and M. Epple, *Angew. Chem., Int. Ed.*, 2013, **52**, 1636–1653.
19 J. Costanza, A. M. El Badawy and T. M. Tolaymat, *Environ. Sci. Technol.*, 2011, **45**, 7591–7592.
20 A. B. Smetana, K. J. Klabunde, G. R. Marchin and C. M. Sorensen, *Langmuir*, 2008, **24**, 7457–7464.
21 A. Pratsinis, P. Hervella, J.-C. Leroux, S. E. Pratsinis and G. A. Sotiriou, *Small*, 2013, **9**, 2576–2584.
22 B. Bellina, R. Antoine, M. Broyer, L. Gell, Z. Sanader, R. Mitric, V. Bonacic-Koutecky and P. Dugourd, *Dalton Trans.*, 2013, **42**, 8328–8333.
23 R. Jin, *Nanoscale*, 2010, **2**, 343–362.
24 D. M. Brewis, I. Mathieson, I. Sutherland, R. A. Cayless and R. H. Dahm, *Int. J. Adhes. Adhes.*, 1996, **16**, 87–95.
25 J. W. Cho and H. Y. Song, *J. Polym. Sci., Part A: Polym. Chem.*, 1995, **33**, 2109–2112.
26 S. De and A. Khan, *Chem. Commun.*, 2012, **48**, 3130–3132.
27 W. D. Benzinger, B. S. Parekh and J. L. Eichelberger, *Sep. Sci. Technol.*, 1980, **15**, 1193–1204.
28 M. G. Buonomenna, P. Macchi, M. Davoli and E. Drioli, *Eur. Polym. J.*, 2007, **43**, 1557–1572.
29 E. Fontananova, J. C. Jansen, A. Cristiano, E. Curcio and E. Drioli, *Desalination*, 2006, **192**, 190–197.
30 K. M. Kim, N.-G. Park, K. S. Ryu and S. H. Chang, *Electrochim. Acta*, 2006, **51**, 5636–5644.
31 H. Matsuyama, M. Teramoto, R. Nakatani and T. Maki, *J. Appl. Polym. Sci.*, 1999, **74**, 171–178.
32 H. Matsuyama, M. Teramoto, R. Nakatani and T. Maki, *J. Appl. Polym. Sci.*, 1999, **74**, 159–170.
33 P. K. S. Mural, M. Sharma, A. Shukla, S. Bhadra, B. Padmanabhan, G. Madras and S. Bose, *RSC Adv.*, 2015, **5**, 32441–32451.
34 M. Sharma, G. Madras and S. Bose, *J. Mater. Chem. A*, 2015, **3**, 5991–6003.
35 J. A. Kharraz, M. R. Bilad and H. A. Arafat, *J. Membr. Sci.*, 2015, **495**, 404–414.
36 R. Thomas, E. Guillen-Burrieza and H. A. Arafat, *J. Membr. Sci.*, 2014, **452**, 470–480.
37 G. J. Ross, J. F. Watts, M. P. Hill and P. Morrissey, *Polymer*, 2000, **41**, 1685–1696.
38 N. A. Rey, O. W. Howarth and E. C. Pereira-Maia, *J. Inorg. Biochem.*, 2004, **98**, 1151–1159.
39 V. S. D. Voet, D. Hermida-Merino, G. ten Brinke and K. Loos, *RSC Adv.*, 2013, **3**, 7938–7946.
40 R. G. Pearson, *J. Am. Chem. Soc.*, 1963, **85**, 3533–3539.
41 S. Zheng, P. Han, Z. Han, H. Zhang, Z. Tang and J. Yang, *Sci. Rep.*, 2014, **4**, 4842.
42 N. Franz, L. Menin and H.-A. Klok, *Org. Biomol. Chem.*, 2009, **7**, 5207–5218.
43 S. Y. Kang and K. Kim, *Langmuir*, 1998, **14**, 226–230.
44 S. Nejati, C. Boo, C. O. Osuji and M. Elimelech, *J. Membr. Sci.*, 2015, **492**, 355–363.
45 F. Huang, Q. Wang, Q. Wei, W. Gao, H. Shou and S. Jiang, *eXPRESS Polym. Lett.*, 2010, **4**, 551–558.
46 W. Zhang, Z. Shi, F. Zhang, X. Liu, J. Jin and L. Jiang, *Adv. Mater.*, 2013, **25**, 2071–2076.
47 T. T. Chau, W. J. Bruckard, P. T. L. Koh and A. V. Nguyen, *Adv. Colloid Interface Sci.*, 2009, **150**, 106–115.
48 C. Beloin, A. Roux and J.-M. Ghigo, *Curr. Top. Microbiol. Immunol.*, 2008, **322**, 249–289.
49 L. Vanysacker, C. Denis, P. Declerck, A. Piasecka and I. F. J. Vankelecom, *BioMed Res. Int.*, 2013, **2013**, 12.
50 T. Nguyen, F. A. Roddick and L. Fan, *Membranes*, 2012, **2**, 804–840.
51 Q. L. Feng, J. Wu, G. Q. Chen, F. Z. Cui, T. N. Kim and J. O. Kim, *J. Biomed. Mater. Res.*, 2000, **52**, 662–668.
52 J. A. Spadaro, T. J. Berger, S. D. Barranco, S. E. Chapin and R. O. Becker, *Antimicrob. Agents Chemother.*, 1974, **6**, 637–642.
53 P. K. Stoimenov, R. L. Klinger, G. L. Marchin and K. J. Klabunde, *Langmuir*, 2002, **18**, 6679–6686.
54 P. K. S. Mural, A. Banerjee, M. S. Rana, A. Shukla, B. Padmanabhan, S. Bhadra, G. Madras and S. Bose, *J. Mater. Chem. A*, 2014, **2**, 17635–17648.
55 Z.-m. Xiu, Q.-b. Zhang, H. L. Puppala, V. L. Colvin and P. J. J. Alvarez, *Nano Lett.*, 2012, **12**, 4271–4275.
56 K. Zodrow, L. Brunet, S. Mahendra, D. Li, A. Zhang, Q. Li and P. J. J. Alvarez, *Water Res.*, 2009, **43**, 715–723.
57 G. M. Nisola, J. S. Park, A. B. Beltran and W.-J. Chung, *RSC Adv.*, 2012, **2**, 2439–2448.